ACS EARTH AND SPACE CHEMISTRY

http://pubs.acs.org/journal/aesccq

Article

The Ocean's Elevator: Evolution of the Air–Seawater Interface during a Small-Scale Algal Bloom

Mickey M. Rogers, Jennifer F. Neal, Ankur Saha, Abdullah S. Algarni, Thomas C. J. Hill, and Heather C. Allen*

Cite This: *ACS Earth Space Chem.* 2020, 4, 2347–2357

Read Online

ACCESS | Metrics & More | Article Recommendations | Supporting Information

ABSTRACT: The composition and lifetime of sea spray aerosols are driven by the molecular and biological complexity of the air–seawater interface. We explore in situ the surface properties of marine algal bloom diatom monocultures by utilizing surface techniques of Brewster angle microscopy (BAM) imaging, vibrational sum-frequency generation (SFG) spectroscopy, and infrared reflection–absorption spectroscopy (IRRAS). Over the course of the bloom, the marine algae produce surface-active biogenic molecules that temporally partition to the topmost interfacial layers and are selectively probed through surface imaging and spectroscopic measurements. BAM images show morphological structural changes and heterogeneity in the interfacial films with increasing density of surface-active biogenic molecules. Film thickness calculations quantified the average surface thickness of a productive bloom over time. The image results reveal an ∼5 nm thick surface region in the late stages of the bloom, which correlates with typical sea surface nanolayer thicknesses. Our surface-specific SFG spectroscopy results show significant diminishing in the intensity of the dangling OH bond of surface water molecules consistent with organic molecules partitioning and replacing water at the air–seawater interface as the algal bloom progresses. Interestingly, we observe a new broad band appear between 3500 and 3600 cm^{-1} in the late stages of the bloom that is attributed to weak hydrogen bonding interactions of water to the surface-active biogenic matter. IRRAS confirms the presence of organic molecules at the surface as we observe an increasing intensity of vibrational alkyl modes and the appearance of a proteinaceous amide band over time. Our work shows the often overlooked but vast potential of tracking changes in the interfacial regime of small-scale laboratory marine algal blooms. By coupling surface imaging and vibrational spectroscopies to complex, time-evolving, marine-relevant systems, we provide additional insight into unraveling the temporal complexity of sea spray aerosol compositions.

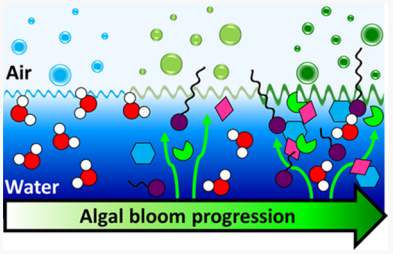

KEYWORDS: *Brewster angle microscopy, algae, film thickness, sum-frequency generation spectroscopy, sea surface nanolayer, sea spray aerosols, marine algal bloom*

INTRODUCTION

Biogenic enrichment at the air–seawater interface occurs throughout the course of a marine algal bloom.[1−4] Marine algae produce proteins, lipids, and carbohydrates, among other surface-active organic molecules that partition to the air–seawater interface and contribute to the composition of the thin layer at the ocean's surface, known as the sea surface microlayer.[5,6] The sea surface microlayer serves as the boundary between the ocean and atmosphere and is therefore crucial to the exchange of gases[7,8] and a wide range of chemical and physical processes in the ocean and atmosphere.[9−11] In addition to this, sea spray aerosols are introduced to the atmosphere through a wave-breaking mechanism at the ocean's surface including bubble entrainment and bursting.[12,13] The changing biogeochemistry of algal systems throughout their bloom alters both sea surface microlayer composition and the mechanics of bubble bursting, giving rise to dynamic changes in sea spray aerosol composition.[4,14−16] In this study, we investigate the marine-relevant diatom *Skeletonema marinoi*,[17] known to produce surface-active organic molecules that include long-chain fatty acids.[2] It is also ice nucleation active.[18] *S. marinoi* was specifically used in this study as it is ubiquitous in temperate coastal seas and is robust in nature, withstanding temperature ranges of 17–22 °C.[19] By tracking molecular and morphological changes at the air–seawater interface, we define the algal bloom as the "ocean's elevator" because it transfers biogenic material from bulk to surface, providing insight into the evolving surface properties throughout the bloom's lifetime.

Diatoms are the most abundant oceanic phytoplankton[20] and exude an abundance of biogenic species over time, including proteins, lipids, and saccharides.[2,21] The behavior of each subset of algal residues in ocean systems have been

Received: August 29, 2020
Revised: November 13, 2020
Accepted: November 24, 2020
Published: December 7, 2020

https://dx.doi.org/10.1021/acsearthspacechem.0c00239
ACS Earth Space Chem. 2020, 4, 2347–2357

reported in the literature, exploring fundamental (one or two component) systems such as protein salt interactions,[22−24] lipid monolayer surfaces (including fatty acids, fatty alcohols, phospholipids, among others),[25,26] and saccharide-enriched interfaces.[3,27] By studying the individual role of each primary subset of algal exudates as demonstrated in the studies above, the fundamental interactions at the ocean's interface and consequent aerosol surfaces can be determined and include interfacial adsorption,[22,27] binding interactions,[28,29] and reaction mechanisms.[30]

Biogenic surfactants have also been explored in more complex systems and have been shown to alter surface features,[31] enhance interactions,[24,25,32,33] and influence the overall film properties.[34] Ex situ analysis of the interfacial regime of native marine systems has been reported, with some studies extending to surface tension measurements,[31] Brewster angle microscopy (BAM),[35,36] and sum-frequency generation (SFG) spectroscopy.[6,37,38] Ex situ BAM imaging studies of highly productive sea surface samples show heterogeneity due to a difference in packing density and the presence of gelatinous macroaggregates of natural films.[35,39,40] Previous work by Laβ et al. using SFG spectroscopy to probe natural marine interfaces showed a significant decrease in the dangling OH of water molecules spanning the air−seawater interface, due to the presence of a film comprised of surface-active biogenic organics such as humic substances, carbohydrate-rich material, proteinaceous material, lipids, and hydrocarbons.[41−43] Laβ et al. suggested the presence of a 1−10 nm natural organic nanolayer, vastly differing from the sea surface microlayer (∼50 μm),[6] comprised of a mixture of organics from marine samples.[43] Consistently, in this work, we show that there is an ∼5 nm thick film produced over the course of the marine algal bloom.

We expand upon these studies by coupling imaging with vibrational spectroscopies in situ. BAM imaging, as well as surface-specific SFG spectroscopy and surface-sensitive infrared reflection−absorption spectroscopy (IRRAS), reveals interfacial structural changes of relevant biogenic processes during a marine algal bloom. The work presented here is conducted in situ to avoid disrupting these often-fragile systems. We track changes throughout the bloom and then calculate trends in film thickness. Ultimately, we provide insights into the dynamic process occurring throughout the bloom and the role of algae as the ocean's elevator, which acts to transfer species between bulk seawater and the air−sea interface. Furthermore, as the algae serve as the ocean's elevator, transporting exudates upward where they will partition to the air−seawater interface, we expect the release of algal species into the aerosol environment. Also, through dry deposition, algal exudates may ultimately be brought back down to the ocean, like a descending elevator. To our knowledge, this is the first BAM imaging and IRRAS study of a small-scale laboratory marine algal bloom in situ.

EXPERIMENTAL SECTION

Materials. *S. marinoi*, Sarno et Zingone (CCMP 2092), a marine diatom, was purchased as an axenic stock culture from the National Center for Marine Algae and Microbiota (NCMA) at Bigelow Laboratory, ME. Filtered seawater (NCMA at Bigelow Laboratory) from the Gulf of Maine, ME with 31−34 ppt salinity was triple bag-filtered through a 1 μm pore size and autoclaved prior to use. Next, the seawater was enriched with nutrients ($NaNO_3$, $NaH_2PO_4{\cdot}H_2O$, $Na_2SiO_3{\cdot}9H_2O$, L1 trace element solution, and f/2 vitamin solution)[44−46] in a 1:1000 mL addition in 1 L Fisherbrand media bottles.

Algae Cultivation for Brewster Angle Microscopy. *S. marinoi* was cultivated in a Teflon Langmuir trough (KSV NIMA, Biolin Scientific, Espoo, Finland, area 148.78 cm^2) for Brewster angle microscopy. Prior to inoculation, the trough was thoroughly cleaned with reagent alcohol (Histological Grade, Fisher Scientific, Fair Lawn, NJ) and ultrapure water with a resistivity of 18.2 MΩ·cm (Milli-Q Advantage A10, EMD Millipore, Billerica, MA). The cleaned trough was filled with nutrient-enriched autoclaved and filtered seawater, inoculated with 1 mL of *S. marinoi* culture and exposed to a 13:11 h day/night cycle (using BlueMax 70 W, Full Spectrum Solutions, MI, 2460 lumens). A water circulator (ISOTEMP 4100C, Fisher Scientific, Inc., PA) was used to control the temperature of the solution in the trough at a constant temperature of 18 °C. The setup was housed in a black Plexiglass box to prevent exposure to dust and other particulate matter. A small top-up of seawater was added to the trough daily to maintain volume, measured with BAM imaging.

Algae Cultivation for Sum-Frequency Generation. *S. marinoi* was cultivated in 9 Erlenmeyer wide-mouth flasks (Pyrex, 250 mL) filled with 100 mL of nutrient-enriched autoclaved and filtered seawater, inoculated with 1 mL of *S. marinoi* algal culture, and capped with autoclaved cheesecloth plugs. The algae flasks were exposed to the same artificial light cycle as described above in a black plexiglass box. A flask was gently swirled, allowed to settle for 2−3 min, and then sampled for sum-frequency generation by pipetting a 10 mL aliquot into a thoroughly cleaned borosilicate glass Petri dish. When pipetting the aliquot, an autoclaved pipet tip was inserted into the mouth of the Erlenmeyer wide-mouth flask into the bulk region, not the bottom, to avoid drawing up algae into the sample, which might induce scattering while taking measurements. For comparison, spectra were obtained immediately after the 5 min acquisition and after a 15 min wait followed by 5 min acquisition to allow for re-establishment of the sea surface layer.[47,48] Once the flask was sampled, it was disposed of to avoid possible contamination in future sampling procedures. The flasks were housed in a black plexiglass box to prevent exposure to dust and other particulate matter.

Algae Cultivation for Infrared Reflection−Absorption Spectroscopy. *S. marinoi* was cultivated in a Teflon Langmuir trough (KSV NIMA, Biolin Scientific, Espoo, Finland, area 144.5 cm^2) with Delrin barriers (KSV NIMA) for infrared reflection−absorption spectroscopy measurements. Prior to inoculation, the trough was thoroughly cleaned with reagent alcohol (Histological Grade, Fisher Scientific, Fair Lawn, NJ) and ultrapure water with a resistivity of 18.2 MΩ·cm (Milli-Q Advantage A10, EMD Millipore, Billerica, MA). The cleaned trough was filled with nutrient-enriched autoclaved and filtered seawater, inoculated with 1 mL of *S. marinoi* culture, and exposed to a 13:11 h day/night cycle (using BlueMax 70 W, Full Spectrum Solutions, MI, 2460 lumens). A water circulator (ISOTEMP 4100C, Fisher Scientific, Inc., PA) was used to control the temperature of the solution in the trough at a constant temperature of 18 °C. The setup was housed in a black plexiglass box to prevent exposure to dust and other particulate matter. A small top-up of seawater was added to the trough daily to maintain volume, measured with infrared reflection−absorption spectroscopy.

https://dx.doi.org/10.1021/acsearthspacechem.0c00239
ACS Earth Space Chem. 2020, 4, 2347−2357

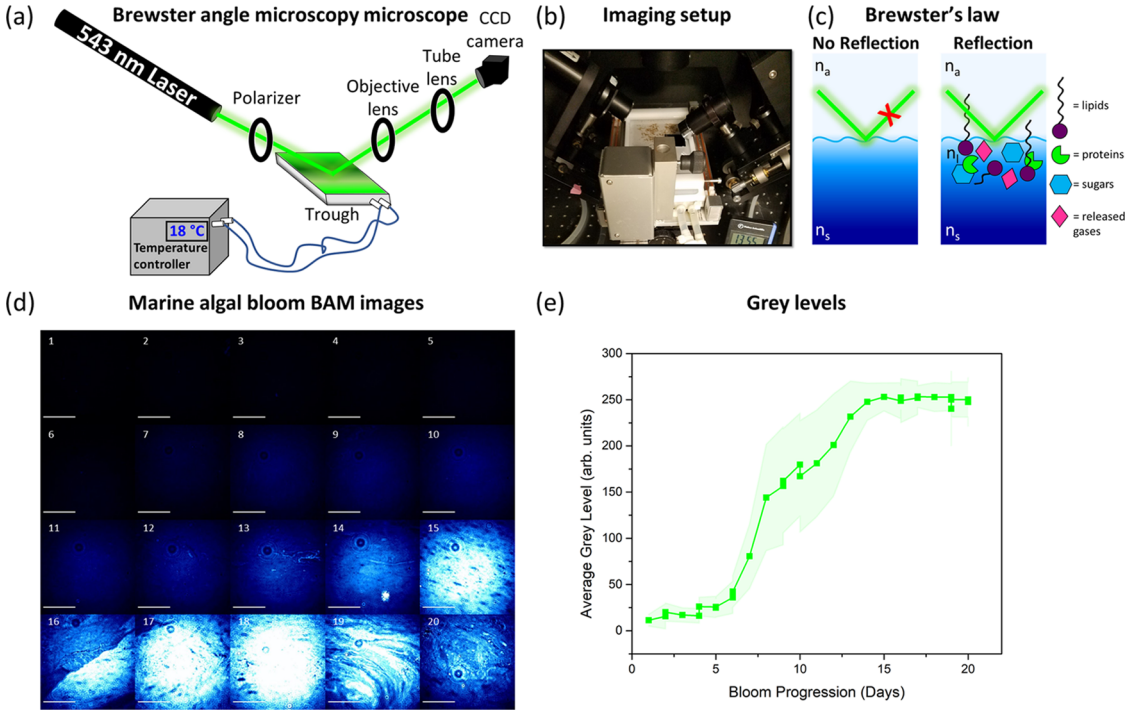

Figure 1. (a) Brewster angle microscope schematic showing the optics diagram, (b) imaging setup, (c) representation of Brewster's law showing no reflection off ocean water at the Brewster angle and light reflecting off the organic-coated surface after the algae have grown, (d) surface images of the marine algal bloom at days 1−20 (day at the top left and 50 μm scale bar at the bottom left, viewable data brightness = 500), and (e) average gray-level value over time.

METHODS

Brewster Angle Microscopy. BAM imaging was performed using a custom-built BAM microscope.[49,50] The BAM microscope is mounted on a goniometer to adjust the angle of incidence to the Brewster angle of an aqueous solution (~53° from the surface normal for pure water). The 1.5 mW He−Ne continuous wave laser source (Research Electro-Optics, Boulder, CO) emits polarized light at 543 nm, which goes through a Glan polarizer, leaving purified p-polarized light to hit and reflect off the aqueous surface.[49] The reflected beam goes through a 10× infinity-corrected superlong working distance objective lens (CFI60 TU Plan EPI, Nikon Instruments, Melville, NY) and a tube lens (MXA22018, Nikon Instruments; focal length 200 mm) to collect and collimate the beam before going into a back-illuminated EM-CCD camera (iXon DV887-BV, Andor Technology, Concord, MA; 512 × 512 active pixels with 16 μm × 16 μm pixel size). The BAM images were processed using ImageJ software and cropped from their original size to show the region of the highest resolution. An artificial blue color scale, with gray-level values ranging from 1−100, was chosen to enhance image contrast. The light and dark blue of the images corresponds to regions with high and low coverage of surface-active species, respectively.

Sum-Frequency Generation Spectroscopy. SFG spectroscopic measurements were obtained using a previously reported setup with minor modifications.[28,51,52] In brief, the output beam from a regenerative Ti:sapphire amplifier (Spitfire Ace, Spectra-Physics) with a sub-50 fs 800 nm pulse is split, where one-half is directed to an optical parametric amplifier (TOPAS-C, Light Conversion) coupled to a noncollinear difference frequency generator (NDFG, Light Conversion) to produce a tunable IR beam, and the other half of the visible beam is spectrally narrowed by an etalon (SLS Optics, United Kingdom). The IR and visible beams are incident onto the sample surface in a copropagating geometry at angles 60 and 50°, respectively, from the surface normal. The SF signal is collected in the reflected direction by a spectrometer (IsoPlane SCT 320, Princeton Instruments) and a liquid nitrogen-cooled CCD (PyLoN, 1340 × 400 pixels, Princeton Instruments). The typical exposure time for one spectrum was 5 min. The spectra were collected in the polarization combination ssp, which describes the polarization of the SF, visible, and IR beams, respectively.

Infrared Reflection−Absorption Spectroscopy. IRRAS spectra were recorded on a Fourier transform infrared (FT-IR) spectrometer (Frontier, Perkin Elmer) equipped with a liquid nitrogen-cooled HgCdTe (MCT) detector previously described.[53,54] Sampling was measured with two aligned gold-plated mirrors (50.8 mm) at an incident angle of 48° from the surface normal. Spectra were recorded as an average of 400 scans in single-beam mode. Spectra were collected under s-polarized light using a polarizer (Thorlabs, ZnSe Holographic Wire Grid Polarizer). Spectra were collected under compressed conditions (from 144.5 to 77.3 cm^2) to concentrate the surface area. Data analysis was processed using Origin software. A third-order polynomial background subtraction was used to fit the data. With the current geometry at an incidence angle of 48°, the peaks are observed as negative bands.

RESULTS AND DISCUSSION

Bloom Progression and Film Thickness by Temporal Surface Imaging. To temporally assess algal bloom progression and the surface partitioning of organic molecules being produced by the bloom, we employed Brewster angle microscopy imaging. Three separate blooms were studied with

https://dx.doi.org/10.1021/acsearthspacechem.0c00239
ACS Earth Space Chem. 2020, 4, 2347−2357

the most productive bloom reported in Figure 1, and the other algal bloom images included in the Supporting Information (SI), Figure S2a,b. Figure 1a−c shows a schematic of the instrument optics, a picture of the settled bloom growing in the imaging setup (Teflon trough), and a diagram explaining Brewster's law, respectively. The defined shapes in Figure 1c in no way represent the proportions of biogenic species, but rather depict the expected exudates likely present in the late stages of the bloom. Reflectivity arises from changes in refractive index from the Brewster angle of the initial solution (i.e., the ocean water) to that of the biogenic film dominating the surface in the late stages of the bloom. The images in Figures 1d and S2a,b show independently grown algal blooms (time in days stated in the top left corner of each image). The dark areas (black and dark blue) of the images correspond to water-rich regions where there is a paucity of surface-active molecular species. There is an observable small round hole in the upper left quadrant, visible starting day 8, which is a physical artifact of our lens and has been normalized for gray scaling. Surface-active algal exudates partition to the air−seawater interface and correspond to the brighter areas (light blue and white) in the image. Our images show that the surface-active biogenic species begin to densely pack at the air−seawater interface, with the onset around day 7. By day 15 of the algal bloom, the images show an intensely bright spot that indicates a possible multilayer of surface-active species, similar to collapse structures of fatty acid films.[26,55,56] Work from Kozarac et al. suggests that natural microlayer samples taken during times of low primary production show homogeneous and continuous images using BAM, whereas periods of high primary production yield granular structures of possible condensed surfactant domains.[40] We observe interesting features in Figure 1d during productive periods on days 15, 16, and 19 specifically, which do not necessarily correlate with a homogeneous film, but we do not believe to be observing surfactant domains, either. Additionally, in Figure S2b, during the late stages (day 11 and onward) of the reported bloom, the BAM reveals seemingly homogeneous and continuous images, similar to the images of original microlayer samples in other work by Kozarac et al.[35] These discrepancies in low and high primary production periods may possibly be due to the in situ measurements employed in our investigation. Figure 1e shows the average gray level of the bloom images over time, demonstrating the utility of using an increasing gray level as a way to track the progress of the bloom. As our small-scale laboratory algal bloom is an axenic system and lacks other planktonic species such as bacteria, the compounds released are limited to the number of productive alga cells, resulting in a noticeable plateauing of gray-level values toward the end of the bloom.

To further understand the algal bloom, we calculated the relative film thickness using the BAM image data in a temporal window during the late stages of the algal bloom (days 7−20). Assuming a constant refractive index, the relative film thickness (d) can be determined from the following relationship,[57] which can model ultrathin films (<20 nm)[58]

$$d = \frac{\lambda\sqrt{R_p}}{\pi \sin(2\theta_B - 90)} \frac{n_l^2(n_a^2 - n_s^2)}{\sqrt{n_a^2 + n_s^2}(n_a^2 - n_l^2)(n_s^2 - n_l^2)} \quad (1)$$

where λ is the laser wavelength, R_p is the p-polarized reflectance, n_l is the refractive index of the marine lipids, and θ_B is the Brewster angle. The refractive indices of air and seawater were parameterized by n_a = 1.00 and n_s = 1.35, respectively.[59] Lower and upper refractive index limits of representative relevant marine algal exudates such as saturated long-chain fatty acids (n_l = 1.430)[60,61] and phospholipids (n_l = 1.478)[62] were used to model film thickness, respectively. With diatoms being the most abundant oceanic phytoplankton,[20] and known for their abundance of lipids and phospholipids, our representative refractive indices are highly relevant.[21,63,64] Moreover, studies show that in strains of *Skeletonema*, in particular, the primary fatty acid is palmitic acid (C16:0).[2] Thus, we selected a saturated long-chain fatty acid's refractive index to model film thickness. Figure 2 shows the temporal evolution of the film thickness throughout the late stages of the bloom (viewable data brightness = 100). The increase in film thickness suggests the release of surface-active organic molecules by productive algae. As the air−seawater interface becomes enriched with biogenic species and begins forming a film, the refractive index at the surface no longer resembles that of the solution but rather the biogenic constituents of the surface film multilayer.

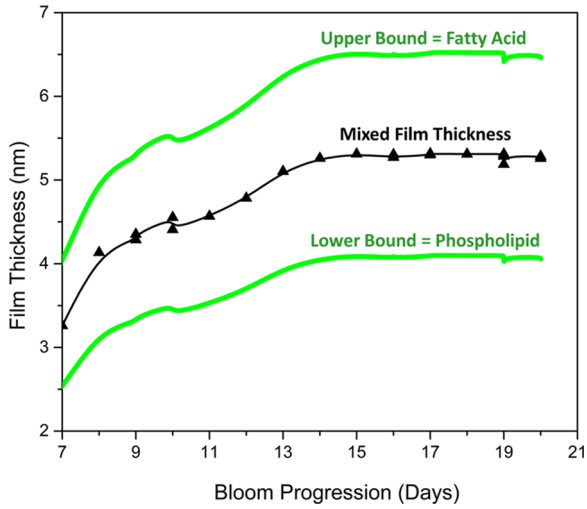

Figure 2. Film thickness (nm) of the late-stage algal bloom versus time (days). The lower and upper bounds are defined by thickness calculations with representative refractive indices (n_l), where the lower limit is n_l = 1.430 (saturated long-chain fatty acid).[60,61] and the upper limit is n_l =1.478 (phospholipid).[62]

The late stages of the algal bloom in Figure 1d reveal an average film thickness of ∼5 nm. While monolayer thickness studies of relevant saturated long-chain fatty acids and phospholipids report average thicknesses ranging from ∼1.6 to 3 nm, depending on the chemical composition of the subphase, our calculated thickness exceeds the monolayer regime suggesting the presence of a multilayer film.[51,62,65] Studies have demonstrated that the sea surface microlayer thickness varies depending on oceanic productivity and sampling technique but averages ∼50 μm.[1,6] There are also studies that suggest the sea surface microlayer is comprised of a separate nanolayer with thicknesses ranging from 2 to 30 nm, which is consistent with our findings.[41,66] Specifically, the "microlayer" is an operative term of the uppermost 0−1000 μm of the sea surface and is often characterized by an enrichment of organics with respect to the underlying water.[38,67] However, the "nanolayer" resembles the typically

https://dx.doi.org/10.1021/acsearthspacechem.0c00239
ACS Earth Space Chem. 2020, 4, 2347−2357

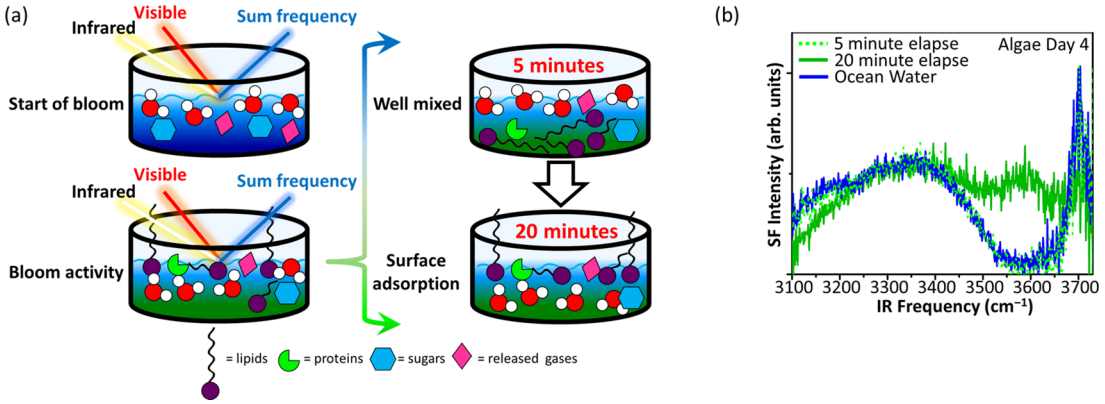

Figure 3. Sum-frequency generation spectroscopy spectra of time-sensitive studies are demonstrated in (a) a schematic representation of the adsorption process of the algae at day 4 growth at 5 and 20 min and (b) spectra after settling in the Petri dish for 5 min (lime green dots), after settling in the Petri dish for 20 min (dark green; time has elapsed such that air−seawater adsorption has occurred, note the enhancement from 3500 to 3600 cm^{-1}), and ocean water (blue) as a control.

surfactant-rich uppermost molecular layers directly at the interface,[42] as we believe we are observing here. We deduce that as the algal bloom progresses, a multilayer film forms yielding increased thickness concurrent with productivity. The morphological variety of these algal blooms is extraordinarily rich, and surface-sensitive methods are necessary for corroborating the presence of surface biogenics in the nanolayer environment.

Interfacial Water Structure Changes during a Marine Algal Bloom. Additional temporal insights into the air−seawater interface and the changing molecular environment of the interface resulting from the progression of an algal bloom can be determined with surface-specific sum-frequency generation (SFG) spectroscopy. SFG spectroscopy is a nonlinear vibrational technique that selectively probes the noncentrosymmetric environment of an interface, such as that studied here—the air−seawater interface. It allows us to track changes in the interfacial hydration environment of a marine algal bloom progressing over time (i.e., at the minute and day timescales). As there is a break in symmetry at the air−seawater interface, we selectively probe the water molecules residing in this interfacial region and find that the water molecules are highly sensitive to the reorganization of the biogenically produced molecules within the interface, thus providing a window into the algal bloom surface properties.

The topmost layers of the ocean contribute to the dynamic composition of sea spray aerosols (SSAs).[68,69] To study the surface layer, we investigate two separate blooms using SFG, reporting on one in both Figures 3 and 4, and the other in Figure S4 to show consistency across blooms. Clearly, by day 4 in the marine algal bloom (Figure 3b), there are enough changes in the water region to impact the composition of SSAs. Interestingly, there is an adsorption time necessary to begin seeing these deviations, as shown schematically in Figure 3a. Figure 3b shows the sum-frequency generation spectroscopy spectra immediately upon transferring the day 4 algae and waiting 5 min for the spectral acquisition. The SFG spectrum immediately after transferring the algae appears to be consistent with the ocean water spectrum. Upon allowing the algae to settle for 20 min (including a 5 min acquisition), we begin to see significant changes. Oceanic waves produce a mixing process of the ocean water. According to Laβ et al., surface sampling yields ∼12.5 times enrichment of surfactants

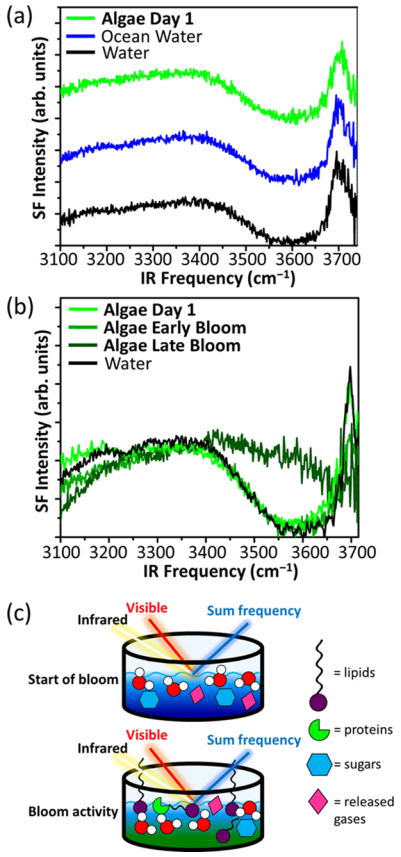

Figure 4. Sum-frequency generation spectra in the water region from 3100 to 3750 cm^{-1} of offset: (a) pure water (black), ocean water (blue), and algae at day 1 growth (light green), (b) algae at day 1 (light green), early bloom (green), late bloom (dark green), and pure water (black), and (c) a schematic representation of interfacial biogenic algal exudates throughout the bloom.

compared to bulk water samples[41,42] and the surface has a renewal process time of several tens of minutes[47] to 1 h.[48]

Figure 4a,b shows our surface-specific spectroscopic results in the vibrational region of water between 3100 and 3750 cm^{-1} in the ssp polarization combination (s: SFG, s: visible, p: infrared). Samples were collected after waiting 20 min (for more detail, see the Experimental Section, Algae cultivation for sum-frequency generation). The spectrum for day 1 algae was

https://dx.doi.org/10.1021/acsearthspacechem.0c00239
ACS Earth Space Chem. 2020, 4, 2347−2357

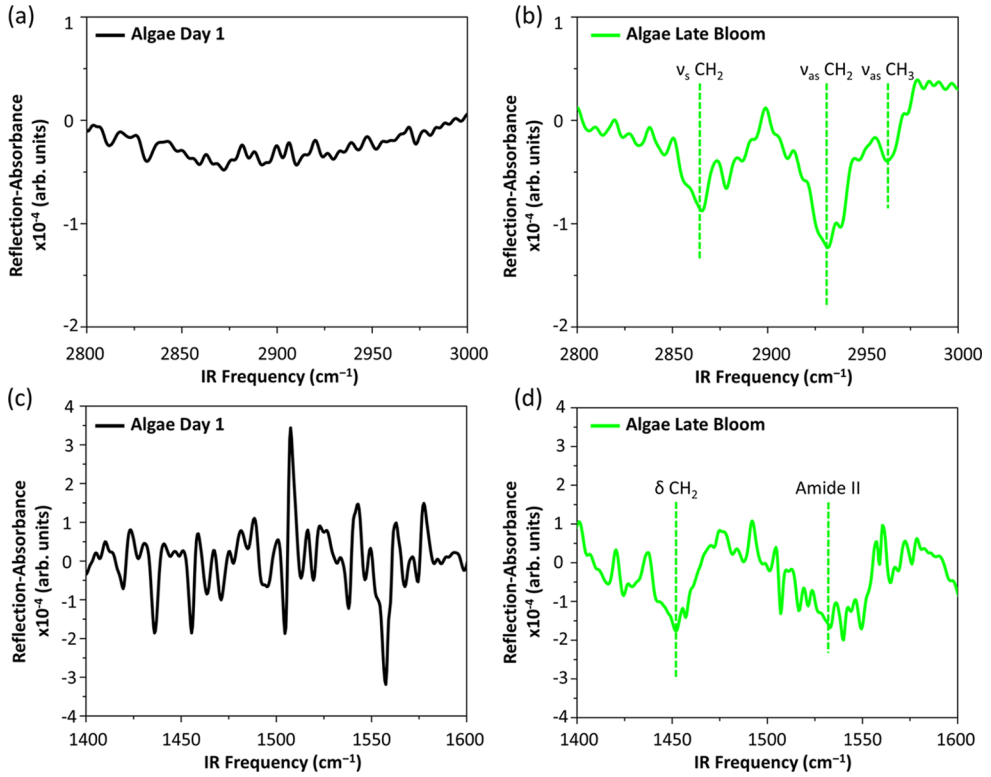

Figure 5. s-Polarized IRRAS spectra, with peaks appearing as negative bands, of (a) day 1 in the alkyl region show a lack of C−H modes (black), (b) day 17 in the alkyl region with the presence of C−H modes (lime green), (c) day 1 in the low-frequency region (black) reveal only noise from incomplete subtraction of water vapor in the beam path, and (d) day 17 in the low-frequency region show the presence of the amide II broad band and the C−H scissoring mode (lime green).

taken multiple times for different bloom cycles to account for bloom onset variation (SI, Figure S4). As seen in Figure 4a, a peak at 3700 cm^{-1} is observed and is attributed to the dangling OH of water molecules pointing up into the air.[29,70] Prior work has established that at the clean water surface, approximately one out of four water molecules contributes to the dangling OH population.[71] The broad band contribution to the region between 3100 and 3600 cm^{-1} corresponds to the hydrogen bonding network of interfacial water, specifically the OH stretching motions of surface water. The band centered at ∼3200 cm^{-1} is attributed to collective symmetric OH stretch motion in a strongly hydrogen-bonded network; the band centered at ∼3450 cm^{-1} is attributed to the OH stretch of water in a more weakly hydrogen-bonded environment.[72−76] There are no significant spectral intensity or frequency differences when comparing the spectra for pure water, ocean water, and algae at day 1 spectra (Figure 4a). There is, however, a small diminishing of the dangling OH peak of water for algae on day 1 as compared to the other spectra. Overall, we observe relatively small deviations for the ocean water and the day 1 algae spectra, indicating that the algae are not producing sufficient surface-active biogenic molecules at this stage to alter the surface water organization, and the chains of algal cells are not surface active.

The spectra and schematic depiction of the algae at the early and late stages of the bloom in Figure 4b,c show a significant deviation relative to the day 1 spectrum in Figure 4a. We find a new and exciting band grow in around ∼3500−3600 cm^{-1} (as seen by Laß et al. at a lower frequency[43]) and a significant diminishing of the free dangling OH of surface water molecules (Figure 4b). We attribute this new band ranging from ∼3500 to 3600 cm^{-1} to weak hydrogen bonding of water molecules to surface-active biological organics as it is consistent with prior work on antifreeze proteins at the surface of water[23] and carboxylic acid headgroups of fatty acids.[29,77] Previous work on natural microlayer samples and their corresponding nanolayers by Laß and Friedrichs also observed a broad OH feature ∼3500 cm^{-1}, which they attribute to the presence of carbohydrate-rich material such as lipopolysaccharides and note the band's increase in intensity during certain times of the year varies with productivity.[42,43] The reduction in the dangling OH is consistent with organic molecules dominating the surface.[78−80] These results are observed across blooms (SI, Figure S4) and correlate with the BAM images (Figure 1d), which show partitioning of algal exudates dominating the air−seawater surface, causing the reduction in the dangling OH.

Organic Partitioning to the Aqueous Surface Using Infrared Reflection−Absorption Spectroscopy. We further explore the interfacial organization at the molecular level during the course of the bloom using surface-sensitive infrared reflection−absorption spectroscopy. IRRAS is a vibrational technique that provides complementary information to the SFG spectra of surface water.[81,82] The benefit of the IRRAS technique is that a large spectral range is collected in a single acquisition from 450 to 4000 cm^{-1}, and the mathematical ratioing in the IRRAS equation (eq 2) provides surface-sensitive information. IRRAS spectra were plotted as reflectance−absorbance (RA)[53,54] which is given as

$$\mathrm{RA} = -\log(R_{\mathrm{alg}}/R_0) \tag{2}$$

where R_{alg} is defined as the reflectivity of the algae and R_0 is the reflectivity of the seawater without algae.

https://dx.doi.org/10.1021/acsearthspacechem.0c00239
ACS Earth Space Chem. 2020, 4, 2347−2357

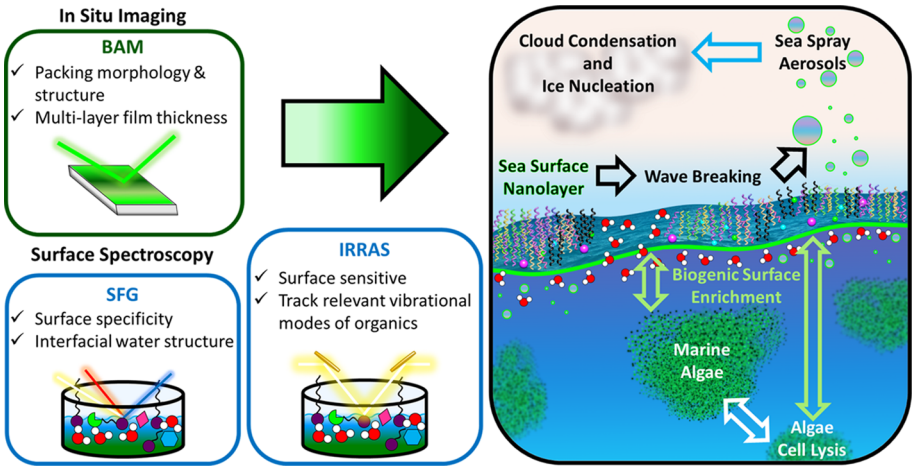

Figure 6. Schematic representation of how our surface techniques (BAM imaging, surface-specific SFG, and surface-sensitive IRRAS) advance understanding of oceanic interfacial evolution, sea spray aerosols, atmospheric nucleation, among other processes.

Figure 5a,b shows the spectra for the early and late stages of the bloom, respectively, in the alkyl stretch region. The peaks, which are present at the late stages in the bloom and absent in early stages, at ∼2963, 2928, and ∼2865 cm^{-1}, correspond to the CH_3-antisymmetric (ν_{as} CH_3), CH_2-antisymmetric (ν_{as} CH_2), and CH_2-symmetric (ν_s CH_2) stretching modes, respectively. The presence of these alkyl modes in the late stages of the bloom confirms surface-active organic enrichment.[53,83] Compared to a well-studied saturated long-chain fatty acid such as palmitic acid, we observe a factor of 10 reduction in the peak intensity of the algal spectrum compared to the condensed phase palmitic acid spectrum in the alkyl region and an ∼14 cm^{-1} blue shift for the CH_2-antisymmetric stretching mode.[30,84,85] The reference sample, palmitic acid, is at a surface concentration of 20 $Å^2$/molecule. The peak shift indicates there are more gauche conformers (more conformational disorder) of the alkyl chains in the algae spectrum compared to the organized fatty acid spectrum (SI, Figure S5).[86−88] Moreover, we collect the IRRAS spectra with s-polarized light (further addressed in the SI, Figure S6), which probes vibrational components lateral to the surface.[89] Our BAM imaging results, shown in Figure 1d, also agree and show the presence of a multilayer film. The multilayer film resembles more of a fatty acid, multilayered, collapse structure, and not a single molecular layer, which would have more trans conformers.

The lower frequency region for both the early and late bloom stages is shown in Figure 5c,d. In the late stage of the bloom, the negative peak at ∼1451 cm^{-1} is assigned to the CH_2 scissoring (δ CH_2) and the negative band at ∼1534 cm^{-1} is assigned to the amide II region. The strong presence of the amide II band indicates the presence of protein.[90−92] The amide II region is commonly present with the amide I peak (∼1651 cm^{-1}) but is overlapping with our OH bend mode (∼1660 cm^{-1}) and not resolvable. Current work is underway to utilize the low-frequency IRRAS spectra for specific chemical identification.

Aerosol Composition and Atmospheric Implications. Serving as an important medium for particle release via bubble bursting,[14] oceanic films have a critical role in impacting local marine environments, as well as global change.[5] Several climate models demonstrate the influence of phytoplankton dynamics on oceanic changes.[93−95] Our study provides insights into how the native, undisturbed, in situ algal bloom behavior may temporally impact aerosol composition and biogeochemical cycles.

As shown in Figure 6, we demonstrate the applicability of studying the ocean's elevator, marine algal blooms, by elucidating molecular changes in surface morphology, film thickness, and interfacial chemical composition. Temporal enhancement of surface-active algal exudates observed by BAM imaging, surface-specific SFG, and surface-sensitive IRRAS vibrational spectroscopies correlate with the evolving chemical composition of the ocean surface and that of sea spray aerosols (SSAs). We demonstrate the applicability of surface imaging and spectroscopic techniques as it provides an important role in the instrumental toolbox for interpreting oceanic and atmospheric changes. As depicted in Figure 6, breaking waves produce entrained air bubbles that surface to the air−seawater interface; the bubbles scavenge biogenic algal exudates, releasing enriched SSA upon bursting.[12−14,96] Thus, following interfacial evolution at the air−seawater interface aids in understanding the sea surface nanolayer, the production and release of SSA, and their role in atmospheric cycles such as cloud and ice formation.[97−99] Recently, work by Ickes et al. reports on the first measurements of ice-nucleating ability of *S. marinoi*, the same species studied in our investigation; aerosol containing *S. marinoi* in a sea spray simulation chamber was ice active.[18] Current work in our lab is underway to identify the chemical composition of the air−seawater interface using additional surface techniques to monitor small-scale laboratory marine algal bloom exudates.

■ CONCLUSIONS

We temporally tracked changes in the air−seawater interface of small-scale laboratory marine algal blooms using a suite of surface imaging and spectroscopic techniques. As the marine algal bloom progresses, Brewster angle microscopy imaging shows that the enhancement of surface-active species dominating the interface and film thickness calculations reveal an increasing thickness for late bloom stages, averaging ∼5 nm thick. Sum-frequency generation spectroscopy reveals significant diminishing in the intensity of the dangling OH of surface waters, which supports the partitioning of algal exudates to the air−seawater interface. Over time, a broad band manifests between 3500 and 3600 cm^{-1}, consistent with weak hydrogen

https://dx.doi.org/10.1021/acsearthspacechem.0c00239
ACS Earth Space Chem. 2020, 4, 2347−2357

bonding networks interacting with organic and biological species. Infrared reflection−absorption spectroscopy spectra also exhibit a temporal increase in the intensity of the alkyl stretch region and the proteinaceous amide band, in accord with natural marine algal bloom growth cycles. Moreover, we begin to unravel the complex role of algae as the ocean's elevator, which acts to transfer biogenics between bulk seawater and the air−seawater interface. To the author's knowledge, this is the first temporal Brewster angle microscopy and infrared reflection−absorption spectroscopy study in situ of small-scale laboratory marine algal blooms.

■ ASSOCIATED CONTENT

Supporting Information

The Supporting Information is available free of charge at https://pubs.acs.org/doi/10.1021/acsearthspacechem.0c00239.

Materials, f/2 vitamin solution recipe, L1 medium recipe, L1 trace element recipe; Experimental details, contamination controls, imaging results reveal temporal change in surface morphology, surface spectroscopy results across independent blooms, and comparison of the algal bloom spectra to ocean relevant fatty acid, palmitic acid (PDF)

■ AUTHOR INFORMATION

Corresponding Author

Heather C. Allen − *Department of Chemistry & Biochemistry, The Ohio State University, Columbus, Ohio 43210, United States;* orcid.org/0000-0003-3120-6784; Phone: +1-614-292-4707; Email: allen@chemistry.ohio-state.edu; Fax: +1-614-292-1685

Authors

Mickey M. Rogers − *Department of Chemistry & Biochemistry, The Ohio State University, Columbus, Ohio 43210, United States*

Jennifer F. Neal − *Department of Chemistry & Biochemistry, The Ohio State University, Columbus, Ohio 43210, United States*

Ankur Saha − *Department of Chemistry & Biochemistry, The Ohio State University, Columbus, Ohio 43210, United States*

Abdullah S. Algarni − *Department of Chemistry & Biochemistry, The Ohio State University, Columbus, Ohio 43210, United States*

Thomas C. J. Hill − *Department of Atmospheric Science, Colorado State University, Fort Collins, Colorado 80523, United States*

Complete contact information is available at: https://pubs.acs.org/10.1021/acsearthspacechem.0c00239

Notes

The authors declare no competing financial interest.

■ ACKNOWLEDGMENTS

We acknowledge support by NSF through the Center for Aerosol Impacts on Chemistry of the Environment (CAICE), CHE-1801971. Data archiving is underway at the UC San Diego Library Digital Collections for CAICE website: https://doi.org/10.6075/J0RR1WRV. The authors declare no competing financial interest. The authors would like to thank K. Carter-Fenk, M. Vazquez de Vasquez, and B. Rogers for insightful comments on the manuscript.

■ REFERENCES

(1) Engel, A.; Sperling, M.; Sun, C.; Grosse, J.; Friedrichs, G. Organic Matter in the Surface Microlayer: Insights From a Wind Wave Channel Experiment. *Front. Mar. Sci.* **2018**, *5*, No. 182.

(2) Jónasdóttir, S. H. Fatty Acid Profiles and Production in Marine Phytoplankton. *Mar. Drugs* **2019**, *17*, No. 151.

(3) Jayarathne, T.; Sultana, C. M.; Lee, C.; Malfatti, F.; Cox, J. L.; Pendergraft, M. A.; Moore, K. A.; Azam, F.; Tivanski, A. V.; Cappa, C. D.; Bertram, T. H.; Grassian, V. H.; Prather, K. A.; Stone, E. A. Enrichment of Saccharides and Divalent Cations in Sea Spray Aerosol During Two Phytoplankton Blooms. *Environ. Sci. Technol.* **2016**, *50*, 11511−11520.

(4) Wang, X.; Sultana, C. M.; Trueblood, J.; Hill, T. C. J.; Malfatti, F.; Lee, C.; Laskina, O.; Moore, K. A.; Beall, C. M.; McCluskey, C. S.; Cornwell, G. C.; Zhou, Y.; Cox, J. L.; Pendergraft, M. A.; Santander, M. V.; Bertram, T. H.; Cappa, C. D.; Azam, F.; DeMott, P. J.; Grassian, V. H.; Prather, K. A. Microbial Control of Sea Spray Aerosol Composition: A Tale of Two Blooms. *ACS Cent. Sci.* **2015**, *1*, 124−131.

(5) Burrows, S. M.; Ogunro, O.; Frossard, A. A.; Russell, L. M.; Rasch, P. J.; Elliott, S. A Physically-Based Framework for Modelling the Organic Fractionation of Sea Spray Aerosol from Bubble Film Langmuir Equilibria. *Atmos. Chem. Phys. Discuss.* **2014**, *14*, 5375−5443.

(6) Engel, A.; Galgani, L. The Organic Sea-Surface Microlayer in the Upwelling Region off the Coast of Peru and Potential Implications for Air−Sea Exchange Processes. *Biogeosciences* **2016**, *13*, 989−1007.

(7) Wurl, O.; Stolle, C.; Van Thuoc, C.; The Thu, P.; Mari, X. Biofilm-like Properties of the Sea Surface and Predicted Effects on Air−Sea CO2 Exchange. *Prog. Oceanogr.* **2016**, *144*, 15−24.

(8) Mustaffa, N. I. H.; Ribas-Ribas, M.; Banko-Kubis, H. M.; Wurl, O. Global Reduction of in Situ CO2 Transfer Velocity by Natural Surfactants in the Sea-Surface Microlayer. *Proc. R. Soc. A* **2020**, *476*, No. 20190763.

(9) Prather, K. A.; Bertram, T. H.; Grassian, V. H.; Deane, G. B.; Stokes, M. D.; DeMott, P. J.; Aluwihare, L. I.; Palenik, B. P.; Azam, F.; Seinfeld, J. H.; Moffet, R. C.; Molina, M. J.; Cappa, C. D.; Geiger, F. M.; Roberts, G. C.; Russell, L. M.; Ault, A. P.; Baltrusaitis, J.; Collins, D. B.; Corrigan, C. E.; Cuadra-Rodriguez, L. A.; Ebben, C. J.; Forestieri, S. D.; Guasco, T. L.; Hersey, S. P.; Kim, M. J.; Lambert, W. F.; Modini, R. L.; Mui, W.; Pedler, B. E.; Ruppel, M. J.; Ryder, O. S.; Schoepp, N. G.; Sullivan, R. C.; Zhao, D. Bringing the Ocean into the Laboratory to Probe the Chemical Complexity of Sea Spray Aerosol. *Proc. Natl. Acad. Sci. U.S.A.* **2013**, *110*, 7550−7555.

(10) Wilson, T. W.; Ladino, L. A.; Alpert, P. A.; Breckels, M. N.; Brooks, I. M.; Browse, J.; Burrows, S. M.; Carslaw, K. S.; Huffman, J. A.; Judd, C.; Kilthau, W. P.; Mason, R. H.; McFiggans, G.; Miller, L. A.; Nájera, J. J.; Polishchuk, E.; Rae, S.; Schiller, C. L.; Si, M.; Temprado, J. V.; Whale, T. F.; Wong, J. P. S.; Wurl, O.; Yakobi-Hancock, J. D.; Abbatt, J. P. D.; Aller, J. Y.; Bertram, A. K.; Knopf, D. A.; Murray, B. J. A Marine Biogenic Source of Atmospheric Ice-Nucleating Particles. *Nature* **2015**, *525*, 234−238.

(11) Irish, V. E.; Hanna, S. J.; Xi, Y.; Boyer, M.; Polishchuk, E.; Ahmed, M.; Chen, J.; Abbatt, J. P. D.; Gosselin, M.; Chang, R.; Miller, L. A.; Bertram, A. K. Revisiting Properties and Concentrations of Ice-Nucleating Particles in the Sea Surface Microlayer and Bulk Seawater in the Canadian Arctic during Summer. *Atmos. Chem. Phys.* **2019**, *19*, 7775−7787.

(12) Blanchard, D. C. The Ejection of Drops from the Sea and Their Enrichment with Bacteria and Other Materials: A Review. *Estuaries* **1989**, *12*, 127−137.

(13) Blanchard, D. C. The Electrification of the Atmosphere by Particles from Bubbles in the Sea. *Prog. Oceanogr.* **1963**, *1*, 73−202.

(14) Wang, X.; Deane, G. B.; Moore, K. A.; Ryder, O. S.; Stokes, M. D.; Beall, C. M.; Collins, D. B.; Santander, M. V.; Burrows, S. M.; Sultana, C. M.; Prather, K. A. The Role of Jet and Film Drops in

Controlling the Mixing State of Submicron Sea Spray Aerosol Particles. *Proc. Natl. Acad. Sci. U.S.A.* **2017**, *114*, 6978−6983.
(15) Lee, C.; Sultana, C. M.; Collins, D. B.; Santander, M. V.; Axson, J. L.; Malfatti, F.; Cornwell, G. C.; Grandquist, J. R.; Deane, G. B.; Stokes, M. D.; Azam, F.; Grassian, V. H.; Prather, K. A. Advancing Model Systems for Fundamental Laboratory Studies of Sea Spray Aerosol Using the Microbial Loop. *J. Phys. Chem. A* **2015**, *119*, 8860−8870.
(16) McCluskey, C. S.; Hill, T. C. J.; Sultana, C. M.; Laskina, O.; Trueblood, J.; Santander, M. V.; Beall, C. M.; Michaud, J. M.; Kreidenweis, S. M.; Prather, K. A.; Grassian, V.; DeMott, P. J. A Mesocosm Double Feature: Insights into the Chemical Makeup of Marine Ice Nucleating Particles. *J. Atmos. Sci.* **2018**, *75*, 2405−2423.
(17) Sarno, D.; Kooistra, W. H. C. F.; Medlin, L. K.; Percopo, I.; Zingone, A. Diversity in the Genus Skeletonema (Bacillariophyceae). Ii. an Assessment of the Taxonomy of *S. costatum*-Like Species with the Description of Four New Species. *J. Phycol.* **2005**, *41*, 151−176.
(18) Ickes, L.; Porter, G. C. E.; Wagner, R.; Adams, M. P.; Bierbauer, S.; Bertram, A. K.; Bilde, M.; Christiansen, S.; Ekman, A. M. L.; Gorokhova, E.; Höhler, K.; Kiselev, A. A.; Leck, C.; Möhler, O.; Murray, B. J.; Schiebel, T.; Ullrich, R.; Salter, M. E. The Ice-Nucleating Activity of Arctic Sea Surface Microlayer Samples and Marine Algal Cultures. *Atmos. Chem. Phys.* **2020**, *20*, 11089−11117.
(19) Lauritano, C.; Carotenuto, Y.; Vitiello, V.; Buttino, I.; Romano, G.; Hwang, J.-S.; Ianora, A. Effects of the Oxylipin-Producing Diatom *Skeletonema marinoi* on Gene Expression Levels of the Calanoid Copepod Calanus Sinicus. *Mar. Genomics* **2015**, *24*, 89−94.
(20) Zulu, N. N.; Zienkiewicz, K.; Vollheyde, K.; Feussner, I. Current Trends to Comprehend Lipid Metabolism in Diatoms. *Prog. Lipid Res.* **2018**, *70*, 1−16.
(21) Vidoudez, C.; Pohnert, G. Comparative Metabolomics of the Diatom *Skeletonema marinoi* in Different Growth Phases. *Metabolomics* **2012**, *8*, 654−669.
(22) Li, Y.; Shrestha, M.; Luo, M.; Sit, I.; Song, M.; Grassian, V. H.; Xiong, W. Salting Up of Proteins at the Air/Water Interface. *Langmuir* **2019**, *35*, 13815−13820.
(23) Meister, K.; Strazdaite, S.; DeVries, A. L.; Lotze, S.; Olijve, L. L. C.; Voets, I. K.; Bakker, H. J. Observation of Ice-like Water Layers at an Aqueous Protein Surface. *Proc. Natl. Acad. Sci. U.S.A.* **2014**, *111*, 17732−17736.
(24) Luo, M.; Dommer, A. C.; Schiffer, J. M.; Rez, D. J.; Mitchell, A. R.; Amaro, R. E.; Grassian, V. H. Surfactant Charge Modulates Structure and Stability of Lipase-Embedded Monolayers at Marine-Relevant Aerosol Surfaces. *Langmuir* **2019**, *35*, 9050−9060.
(25) Neal, J. F.; Rogers, M. M.; Smeltzer, M. A.; Carter-Fenk, K. A.; Grooms, A. J.; Zerkle, M. M.; Allen, H. C. Sodium Drives Interfacial Equilibria for Semi-Soluble Phosphoric and Phosphonic Acids of Model Sea Spray Aerosol Surfaces. *ACS Earth Space Chem.* **2020**, *4*, 1549−1557.
(26) Carter-Fenk, K. A.; Allen, H. C. Collapse Mechanisms of Nascent and Aged Sea Spray Aerosol Proxy Films. *Atmosphere* **2018**, *9*, No. 503.
(27) Hasenecz, E. S.; Kaluarachchi, C. P.; Lee, H. D.; Tivanski, A. V.; Stone, E. A. Saccharide Transfer to Sea Spray Aerosol Enhanced by Surface Activity, Calcium, and Protein Interactions. *ACS Earth Space Chem.* **2019**, *3*, 2539−2548.
(28) Adams, E. M.; Wellen, B. A.; Thiraux, R.; Reddy, S. K.; Vidalis, A. S.; Paesani, F.; Allen, H. C. Sodium−Carboxylate Contact Ion Pair Formation Induces Stabilization of Palmitic Acid Monolayers at High PH. *Phys. Chem. Chem. Phys.* **2017**, *19*, 10481−10490.
(29) Hua, W.; Verreault, D.; Huang, Z.; Adams, E. M.; Allen, H. C. Cation Effects on Interfacial Water Organization of Aqueous Chloride Solutions. I. Monovalent Cations: Li^+, Na^+, K^+, and NH_4^+. *J. Phys. Chem. B* **2014**, *118*, 8433−8440.
(30) Shrestha, M.; Luo, M.; Li, Y.; Xiang, B.; Xiong, W.; Grassian, V. H. Let There Be Light: Stability of Palmitic Acid Monolayers at the Air/Salt Water Interface in the Presence and Absence of Simulated Solar Light and a Photosensitizer. *Chem. Sci.* **2018**, *9*, 5716−5723.
(31) Lee, H. D.; Morris, H. S.; Laskina, O.; Sultana, C. M.; Lee, C.; Jayarathne, T.; Cox, J. L.; Wang, X.; Hasenecz, E. S.; DeMott, P. J.; Bertram, T. H.; Cappa, C. D.; Stone, E. A.; Prather, K. A.; Grassian, V. H.; Tivanski, A. V. Organic Enrichment, Physical Phase State, and Surface Tension Depression of Nascent Core−Shell Sea Spray Aerosols during Two Phytoplankton Blooms. *ACS Earth Space Chem.* **2020**, *4*, 650−660.
(32) Schiffer, J. M.; Luo, M.; Dommer, A. C.; Thoron, G.; Pendergraft, M.; Santander, M. V.; Lucero, D.; Pecora de Barros, E.; Prather, K. A.; Grassian, V. H.; Amaro, R. E. Impacts of Lipase Enzyme on the Surface Properties of Marine Aerosols. *J. Phys. Chem. Lett.* **2018**, *9*, 3839−3849.
(33) Burrows, S. M.; Gobrogge, E.; Fu, L.; Link, K.; Elliott, S. M.; Wang, H.; Walker, R. OCEANFILMS-2: Representing Coadsorption of Saccharides in Marine Films and Potential Impacts on Modeled Marine Aerosol Chemistry. *Geophys. Res. Lett.* **2016**, *43*, 8306−8313.
(34) Farajzadeh, R.; Krastev, R.; Zitha, P. L. J. Foam Film Permeability: Theory and Experiment. *Adv. Colloid Interface Sci.* **2008**, *137*, 27−44.
(35) Kozarac, Z.; Risović, D.; Frka, S.; Möbius, D. Reflection of Light from the Air/Water Interface Covered with Sea-Surface Microlayers. *Mar. Chem.* **2005**, *96*, 99−113.
(36) Kozarac, Z.; Möbius, D.; Spohn, D. B. Investigation of Sea-Surface Microlayer and Phytoplankton Culture Samples by Monolayer Techniques and Brewster Angle Microscopy. *Croat. Chem. Acta* **1998**, *71*, 285−301.
(37) Engel, A.; Bange, H. W.; Cunliffe, M.; Burrows, S. M.; Friedrichs, G.; Galgani, L.; Herrmann, H.; Hertkorn, N.; Johnson, M.; Liss, P. S.; Quinn, P. K.; Schartau, M.; Soloviev, A.; Stolle, C.; Upstill-Goddard, R. C.; van Pinxteren, M.; Zäncker, B. The Ocean's Vital Skin: Toward an Integrated Understanding of the Sea Surface Microlayer. *Front. Mar. Sci.* **2017**, *4*, No. 165.
(38) Engel, A.; Sperling, M.; Sun, C.; Grosse, J.; Friedrichs, G. Organic Matter in the Surface Microlayer: Insights From a Wind Wave Channel Experiment. *Front. Mar. Sci.* **2018**, *5*, No. 182.
(39) Gašparović, B.; Kozarac, Z.; Saliot, A.; Ćosović, B.; Möbius, D. Physicochemical Characterization of Natural Andex-SituReconstructed Sea-Surface Microlayers. *J. Colloid Interface Sci.* **1998**, *208*, 191−202.
(40) Kozarac, Z.; Möbius, D.; Romero, M. T. M. Characterization of Aquatic Natural Microlayers by Monolayer Techniques and Brewster Angle Microscopy. *Water Res.* **2000**, *34*, 1463−1472.
(41) Laβ, K.; Kleber, J.; Friedrichs, G. Vibrational Sum-Frequency Generation as a Probe for Composition, Chemical Reactivity, and Film Formation Dynamics of the Sea Surface Nanolayer. *Limnol. Oceanogr.: Methods* **2010**, *8*, 216−228.
(42) Laß, K.; Friedrichs, G. Revealing Structural Properties of the Marine Nanolayer from Vibrational Sum Frequency Generation Spectra *J. Geophys. Res. Oceans* 2011, *116* (C8), C08042, DOI: 10.1029/2010JC006609.
(43) Laß, K.; Bange, H. W.; Friedrichs, G. Seasonal Signatures in SFG Vibrational Spectra of the Sea Surface Nanolayer at Boknis Eck Time Series Station (SW Baltic Sea). *Biogeosciences* **2013**, *10*, 5325−5334.
(44) Guillard, R. R. L. Culture of Phytoplankton for Feeding Marine Invertebrates. In *Culture of Marine Invertebrate Animals: Proceedings — 1st Conference on Culture of Marine Invertebrate Animals Greenport*;- Smith, W. L.; Chanley, M. H., Eds.; Springer: Boston, M. A., 1975; pp 29−60.
(45) Guillard, R. R. L.; Ryther, J. H. Studies of Marine Planktonic Diatoms: I. Cyclotella Nana Hustedt, and Detonula Confervacea (Cleve) Gran. *Can. J. Microbiol.* **1962**, *8*, 229−239.
(46) Guillard, R. R. L.; Hargraves, P. E. Stichochrysis Immobilis Is a Diatom, Not a Chrysophyte. *Phycologia* **1993**, *32*, 234−236.
(47) Frew, N. M. The Role of Organic Films in Air−Sea Gas Exchange. In *The Sea Surface and Global Change*; Liss, P. S.; Duce, R. A., Eds.; Cambridge University Press: Cambridge, 1997; pp 121−172.

(48) Schmidt, R. Einfluss Natürlicher Organischer Filme Auf Den Gasaustausch Zwischen Meer Und Atmosphäre, Doctoral Dissertation Universität Rostock, 2009.
(49) Neal, J. F.; Zhao, W.; Grooms, A. J.; Flood, A. H.; Allen, H. C. Arginine−Phosphate Recognition Enhanced in Phospholipid Monolayers at Aqueous Interfaces. *J. Phys. Chem. C* **2018**, *122*, 26362−26371.
(50) Adams, E. M.; Allen, H. C. Palmitic Acid on Salt Subphases and in Mixed Monolayers of Cerebrosides: Application to Atmospheric Aerosol Chemistry. *Atmosphere* **2013**, *4*, 315−336.
(51) Adams, E. M.; Verreault, D.; Jayarathne, T.; Cochran, R. E.; Stone, E. A.; Allen, H. C. Surface Organization of a DPPC Monolayer on Concentrated $SrCl_2$ and $ZnCl_2$ Solutions. *Phys. Chem. Chem. Phys.* **2016**, *18*, 32345−32357.
(52) Lin, L.; Husek, J.; Biswas, S.; Baumler, S. M.; Adel, T.; Ng, K. C.; Baker, L. R.; Allen, H. C. Iron(III) Speciation Observed at Aqueous and Glycerol Surfaces: Vibrational Sum Frequency and X-Ray. *J. Am. Chem. Soc.* **2019**, *141*, 13525−13535.
(53) Neal, J. F.; Zhao, W.; Grooms, A. J.; Smeltzer, M. A.; Shook, B. M.; Flood, A. H.; Allen, H. C. Interfacial Supramolecular Structures of Amphiphilic Receptors Drive Aqueous Phosphate Recognition. *J. Am. Chem. Soc.* **2019**, *141*, 7876−7886.
(54) Grooms, A. J.; Neal, J. F.; Ng, K. C.; Zhao, W.; Flood, A. H.; Allen, H. C. Thermodynamic Signatures of the Origin of Anti-Hofmeister Selectivity for Phosphate at Aqueous Interfaces. *J. Phys. Chem. A* **2020**, *124*, 5621−5630.
(55) Lee, K. Y. C. Collapse Mechanisms of Langmuir Monolayers. *Annu. Rev. Phys. Chem.* **2008**, *59*, 771−791.
(56) McFate, C.; Ward, D.; Olmsted, J. Organized Collapse of Fatty Acid Monolayers. *Langmuir* **1993**, *9*, 1036−1039.
(57) Pusterla, J. M.; Malfatti-Gasperini, A. A.; Puentes-Martinez, X. E.; Cavalcanti, L. P.; Oliveira, R. G. Refractive Index and Thickness Determination in Langmuir Monolayers of Myelin Lipids. *Biochim. Biophys. Acta, Biomembr.* **2017**, *1859*, 924−930.
(58) Winsel, K.; Hönig, D.; Lunkenheimer, K.; Geggel, K.; Witt, C. Quantitative Brewster Angle Microscopy of the Surface Film of Human Broncho-Alveolar Lavage Fluid. *Eur. Biophys. J* **2003**, *32*, 544−552.
(59) Austin, R. W.; Halikas, G. *The Index of Refraction of Seawater*; Defense Technical Information Center: Fort Belvoir, VA, 1976.
(60) Ayoub, G. T.; Bashara, N. M. Characterization of a Very Thin Uniaxial Film on a Nonabsorbing Substrate by Multiple Wavelength Ellipsometry: Palmitic Acid on Water*. *J. Opt. Soc. Am.* **1978**, *68*, 978−983.
(61) Craig, B. M. Refractive Indices of Some Saturated and Monoethenoid Fatty Acids and Methyl Esters. *Can. J. Chem.* **1953**, *31*, 499−504.
(62) Kienle, D. F.; de Souza, J. V.; Watkins, E. B.; Kuhl, T. L. Thickness and Refractive Index of DPPC and DPPE Monolayers by Multiple-Beam Interferometry. *Anal. Bioanal. Chem.* **2014**, *406*, 4725−4733.
(63) Obata, T.; Fernie, A. R.; Nunes-Nesi, A. The Central Carbon and Energy Metabolism of Marine Diatoms. *Metabolites* **2013**, *3*, 325−346.
(64) Geider, R.; Roche, J. L. Redfield Revisited: Variability of C:N:P in Marine Microalgae and Its Biochemical Basis. *Eur. J. Phycol.* **2002**, *37*, 1−17.
(65) Reynolds, P. A.; McGillivray, D. J.; Gilbert, E. P.; Holt, S. A.; Henderson, M. J.; White, J. W. Neutron and X-Ray Reflectivity from Polyisobutylene-Based Amphiphiles at the Air−Water Interface. *Langmuir* **2003**, *19*, 752−761.
(66) Hunter, K. A.; Liss, P. S. Chapter 9 Organic Sea Surface Films. In *Marine Organic Chemistry*;Duursma, E. K.; Dawson, R., Eds.; Elsevier Oceanography Series; Elsevier, 1981; Vol. *31*, pp 259−298.
(67) Hunter, K. A. Processes Affecting Particulate Trace Metals in the Sea Surface Microlayer. *Mar. Chem.* **1980**, *9*, 49−70.
(68) Quinn, P. K.; Collins, D. B.; Grassian, V. H.; Prather, K. A.; Bates, T. S. Chemistry and Related Properties of Freshly Emitted Sea Spray Aerosol. *Chem. Rev.* **2015**, *115*, 4383−4399.
(69) Cochran, R. E.; Laskina, O.; Jayarathne, T.; Laskin, A.; Laskin, J.; Lin, P.; Sultana, C.; Lee, C.; Moore, K. A.; Cappa, C. D.; Bertram, T. H.; Prather, K. A.; Grassian, V. H.; Stone, E. A. Analysis of Organic Anionic Surfactants in Fine and Coarse Fractions of Freshly Emitted Sea Spray Aerosol. *Environ. Sci. Technol.* **2016**, *50*, 2477−2486.
(70) Brown, M. G.; Walker, D. S.; Raymond, E. A.; Richmond, G. L. Vibrational Sum-Frequency Spectroscopy of Alkane/Water Interfaces: Experiment and Theoretical Simulation. *J. Phys. Chem. B* **2003**, *107*, 237−244.
(71) Shen, Y. R. 1998 Frank Isakson Prize Address Sum Frequency Generation for Vibrational Spectroscopy: Applications to Water Interfaces and Films of Water and Ice. *Solid State Commum.* **1998**, *108*, 399−406.
(72) Gragson, D. E.; Richmond, G. L. Investigations of the Structure and Hydrogen Bonding of Water Molecules at Liquid Surfaces by Vibrational Sum Frequency Spectroscopy. *J. Phys. Chem. B* **1998**, *102*, 3847−3861.
(73) Gragson, D. E.; Richmond, G. L. Probing the Intermolecular Hydrogen Bonding of Water Molecules at the CCl4/Water Interface in the Presence of Charged Soluble Surfactant. *J. Chem. Phys.* **1997**, *107*, 9687−9690.
(74) Walker, R. A.; Gruetzmacher, J. A.; Richmond, G. L. Phosphatidylcholine Monolayer Structure at a Liquid−Liquid Interface. *J. Am. Chem. Soc.* **1998**, *120*, 6991−7003.
(75) Sovago, M.; Kramer Campen, R.; Bakker, H. J.; Bonn, M. Hydrogen Bonding Strength of Interfacial Water Determined with Surface Sum-Frequency Generation. *Chem. Phys. Lett.* **2009**, *470*, 7−12.
(76) Dalchand, N.; Doğangün, M.; Ohno, P. E.; Ma, E.; Martinson, A. B. F.; Geiger, F. M. Perturbation of Hydrogen-Bonding Networks over Supported Lipid Bilayers by Poly(Allylamine Hydrochloride). *J. Phys. Chem. B* **2019**, *123*, 4251−4257.
(77) Chen, X.; Hua, W.; Huang, Z.; Allen, H. C. Interfacial Water Structure Associated with Phospholipid Membranes Studied by Phase-Sensitive Vibrational Sum Frequency Generation Spectroscopy. *J. Am. Chem. Soc.* **2010**, *132*, 11336−11342.
(78) Tang, C. Y.; Huang, Z.; Allen, H. C. Interfacial Water Structure and Effects of Mg2+ and Ca2+ Binding to the COOH Headgroup of a Palmitic Acid Monolayer Studied by Sum Frequency Spectroscopy. *J. Phys. Chem. B* **2011**, *115*, 34−40.
(79) Ma, G.; Chen, X.; Allen, H. C. Dangling OD Confined in a Langmuir Monolayer. *J. Am. Chem. Soc.* **2007**, *129*, 14053−14057.
(80) Shen, Y. R.; Ostroverkhov, V. Sum-Frequency Vibrational Spectroscopy on Water Interfaces: Polar Orientation of Water Molecules at Interfaces. *Chem. Rev.* **2006**, *106*, 1140−1154.
(81) Griffith, E. C.; Vaida, V. Ionization State of L-Phenylalanine at the Air−Water Interface. *J. Am. Chem. Soc.* **2013**, *135*, 710−716.
(82) Griffith, E. C.; Adams, E. M.; Allen, H. C.; Vaida, V. Hydrophobic Collapse of a Stearic Acid Film by Adsorbed L-Phenylalanine at the Air−Water Interface. *J. Phys. Chem. B* **2012**, *116*, 7849−7857.
(83) Woden, B.; Skoda, M.; Hagreen, M.; Pfrang, C. Night-Time Oxidation of a Monolayer Model for the Air−Water Interface of Marine Aerosols—A Study by Simultaneous Neutron Reflectometry and in Situ Infra-Red Reflection Absorption Spectroscopy (IRRAS). *Atmosphere* **2018**, *9*, 471.
(84) Rudd, B. A. W.; Vidalis, A. S.; Allen, H. C. Thermodynamic versus Non-Equilibrium Stability of Palmitic Acid Monolayers in Calcium-Enriched Sea Spray Aerosol Proxy Systems. *Phys. Chem. Chem. Phys.* **2018**, *20*, 16320−16332.
(85) Griffith, E. C.; Vaida, V. In Situ Observation of Peptide Bond Formation at the Water-Air Interface. *Proc. Natl. Acad. Sci. U.S.A.* **2012**, *109*, 15697−15701.
(86) Bensebaa, F.; Ellis, T. H.; Badia, A.; Lennox, R. B. Thermal Treatment of N-Alkanethiolate Monolayers on Gold, As Observed by Infrared Spectroscopy. *Langmuir* **1998**, *14*, 2361−2367.
(87) Du, X.; Miao, W.; Liang, Y. IRRAS Studies on Chain Orientation in the Monolayers of Amino Acid Amphiphiles at the Air−Water Interface Depending on Metal Complex and Hydrogen

Bond Formation with the Headgroups. *J. Phys. Chem. B* **2005**, *109*, 7428−7434.
(88) Cieślik-Boczula, K.; Czarnik-Matusewicz, B.; Perevozkina, M.; Filarowski, A.; Boens, N.; De Borggraeve, W. M.; Koll, A. ATR-IR Spectroscopic Study of the Structural Changes in the Hydrophobic Region of ICPAN/DPPC Bilayers. *J. Mol. Struct.* **2008**, *878*, 162−168.
(89) Mendelsohn, R.; Mao, G.; Flach, C. R. Infrared Reflection−Absorption Spectroscopy: Principles and Applications to Lipid−Protein Interaction in Langmuir Films. *Biochim. Biophys. Acta, Biomembr.* **2010**, *1798*, 788−800.
(90) Mendelsohn, R.; Brauner, J. W.; Gericke, A. External Infrared Reflection Absorption Spectrometry of Monolayer Films at the Air-Water Interface. *Annu. Rev. Phys. Chem.* **1995**, *46*, 305−334.
(91) de Brito, A. K.; Caseli, L.; Nordi, C. S. F. Algal Polysaccharides on Lipid Langmuir−Blodgett Films and Molecular Effects upon Metal Ion Contact. *Thin Solid Films* **2013**, *534*, 312−315.
(92) Dousseau, F.; Pezolet, M. Determination of the Secondary Structure Content of Proteins in Aqueous Solutions from Their Amide I and Amide II Infrared Bands. Comparison between Classical and Partial Least-Squares Methods. *Biochemistry* **1990**, *29*, 8771−8779.
(93) Boyd, P. W.; Doney, S. C.; Strzepek, R.; Dusenberry, J.; Lindsay, K.; Fung, I. Climate-Mediated Changes to Mixed-Layer Properties in the Southern Ocean: Assessing the Phytoplankton Response. *Biogeosciences* **2008**, *5*, 847−864.
(94) Elliott, J. A.; Thackeray, S. J.; Huntingford, C.; Jones, R. G. Combining a Regional Climate Model with a Phytoplankton Community Model to Predict Future Changes in Phytoplankton in Lakes. *Freshwater Biol.* **2005**, *50*, 1404−1411.
(95) Bullerjahn, G. S.; McKay, R. M.; Davis, T. W.; Baker, D. B.; Boyer, G. L.; D'Anglada, L. V.; Doucette, G. J.; Ho, J. C.; Irwin, E. G.; Kling, C. L.; Kudela, R. M.; Kurmayer, R.; Michalak, A. M.; Ortiz, J. D.; Otten, T. G.; Paerl, H. W.; Qin, B.; Sohngen, B. L.; Stumpf, R. P.; Visser, P. M.; Wilhelm, S. W. Global Solutions to Regional Problems: Collecting Global Expertise to Address the Problem of Harmful Cyanobacterial Blooms. A Lake Erie Case Study. *Harmful Algae* **2016**, *54*, 223−238.
(96) Aller, J. Y.; Radway, J. C.; Kilthau, W. P.; Bothe, D. W.; Wilson, T. W.; Vaillancourt, R. D.; Quinn, P. K.; Coffman, D. J.; Murray, B. J.; Knopf, D. A. Size-Resolved Characterization of the Polysaccharidic and Proteinaceous Components of Sea Spray Aerosol. *Atmos. Environ.* **2017**, *154*, 331−347.
(97) Collins, D. B.; Bertram, T. H.; Sultana, C. M.; Lee, C.; Axson, J. L.; Prather, K. A. Phytoplankton Blooms Weakly Influence the Cloud Forming Ability of Sea Spray Aerosol. *Geophys. Res. Lett.* **2016**, *43*, 9975−9983.
(98) DeMott, P. J.; Mason, R. H.; McCluskey, C. S.; Hill, T. C. J.; Perkins, R. J.; Desyaterik, Y.; Bertram, A. K.; Trueblood, J. V.; Grassian, V. H.; Qiu, Y.; Molinero, V.; Tobo, Y.; Sultana, C. M.; Lee, C.; Prather, K. A. Ice Nucleation by Particles Containing Long-Chain Fatty Acids of Relevance to Freezing by Sea Spray Aerosols. *Environ. Sci.: Processes Impacts* **2018**, *20*, 1559−1569.
(99) Ebben, C. J.; Ault, A. P.; Ruppel, M. J.; Ryder, O. S.; Bertram, T. H.; Grassian, V. H.; Prather, K. A.; Geiger, F. M. Size-Resolved Sea Spray Aerosol Particles Studied by Vibrational Sum Frequency Generation. *J. Phys. Chem. A* **2013**, *117*, 6589−6601.

https://dx.doi.org/10.1021/acsearthspacechem.0c00239
ACS Earth Space Chem. 2020, 4, 2347−2357